Original Research Article

Modeling heat transfers in a typical roasting oven of Burkina Faso

ABSTRACT

This work concerns a numerical study of heat transfers in a typical roasting oven in Burkina Faso. The numerical methodology is based on the nodal method and the heat transfer equations have been established by performing a heat balance on each node. The equations obtained were then discretized using an implicit finite difference scheme and solved by the Gauss algorithm. The numerical results validated by the experiment show that the heat transfers within the oven are mainly influenced by the gas flow, the ambient temperature, the flame extinction time and the wind speed. Increasing gas flow rate and increasing ambient temperature increase the oven cavity temperature. The increase in wind speed causes a significant drop in the oven cavity temperature after the first 15 minutes of operation. Beyond a wind speed of 3m/s, we observe a convergence of the oven cavity temperatures towards a limit value. Regardless of the time the flame is extinguished, the gas flow rate, the ambient temperature and the wind speed, the oven cavity temperature drops rapidly towards the ambient temperature.

Keywords: Roasting oven, nodal modeling, heat transfer, oven cavity temperature, energy losses

1. INTRODUCTION

Burkina Faso, many meat processing equipment are used among which wood and charcoal furnaces, as well as roasters operating with wood and gas. However, most of these equipment are made by local artisans without knowledge of quality issues. In our previous work, we conducted scientific studies to verify the quality of these equipment. The results actually showed that these equipment had poor energy efficiency. Indeed, the charcoal ovens lose (by convection and radiation) almost half of the fuel consumed essentially through their non-isolated metal walls and their yield is in the range 15-17%, comparable to that of traditional fireplaces (FT) [1]. When to the wooden roasters, their yield is of the order of 19%, also comparable to that of FT [2]. The yield of gas roasters is of the order of 35% [3], which is still below the recommended standards for this type of oven (40-50%). Given the above results highlighting the low energy efficiency of equipment, we have undertaken scientific work of optimizing different equipment starting with the charcoal oven [4, 5, 6]. In these optimization works, we used numerical methods as a first step in order to have simulated data of the basic prototype. Then on the basis of the digital code obtained, an optimization model has been developed and implemented. The results obtained then allowed to develop optimized prototypes [7]. In the literature, several works showed the importance of numerical methods in the study and optimization of roasters performance [8,9,10,11]. The modeling methods used differ according to the objectives of the studies. They can be CFD type [12,13] , zonal [14] or nodal [15]. Also, the objective of this work is to model and simulate a typical roaster prototype of Burkina Faso using nodal modeling method. The influence of parameters such as gas flow rate, wind speed, ambient temperature, extinguishing time on oven operation will be analyzed in detail. The data and numerical code obtained will be used later to carry out prototype optimization work.

2. PROBLEM FORMULATION

2.1. Physical Model

Most of the locally made metal ovens are used in pork rotisserie. Most of this equipment is not insulated and works with wood. However, to have a regularity of heat flow, gas will be used instead of wood as an energy source. The prototype retained for the study is therefore almost the same as that used in our study on the energy efficiency of gas oven [3]. Only

here we will not take into account the insulation of the oven, as is the case in the most roasting ovens. Fig. 1 show the oven physical model.

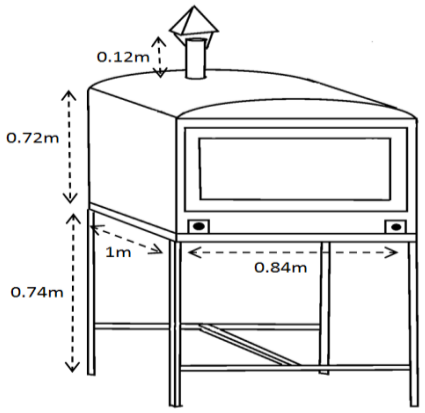

Fig.1: Diagram of the roasting oven

2.2. Mathematical Formulation

Using an oven involves transferring heat to a load (food) in order to raise its temperature. These heat transfers, which are of three types (convection, conduction and radiation) take place simultaneously throughout the cooking time, but in different proportions. To complete our work we adopt the following simplifying assumptions:

- The thermo-physical properties of materials are considered constant during the firing operation ;
- At constant gas flow rate the temperature distribution is assumed to be homogeneous inside the oven;
-
- The thermal properties of the air inside and outside the oven depend on temperature changes.

Determining the overall thermal behavior of the roasting oven consists of determining the thermal behavior of the different nodes representing the different parts of the equipment as shown in fig. 2.

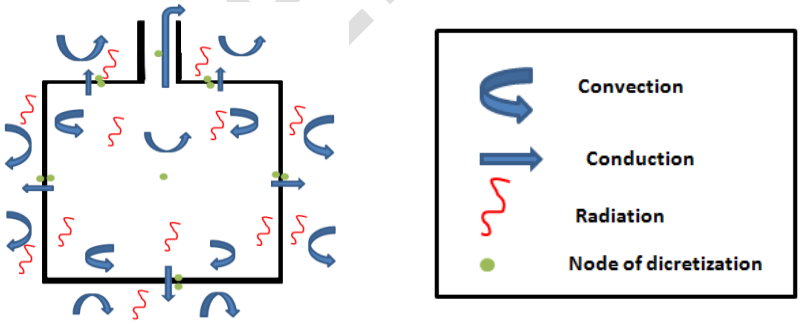

Fig.2: Roasting oven heat transfer model and discretization

In general, in each node we have the following equation [16].

$$\rho_i V_i C_i \frac{\partial T}{\partial t} = \sum_{i=1}^{n}\sum_{i=1}^{m} k_{i,j}\left(T_j - T_i\right) + Q + m_{air} h_{air}^{e} - m_{air} h_{air}^{s} \quad (1)$$

ρ_i : Density of the node i en (m^3/ kg)

V_i: Volume of the node i

C_i: Thermal heat capacity ($J.Kg^{-1}.K^{-1}$)

K_{ij} : Thermal conductance of nodes i and j ($W.K^{-1}$)

m_{air} : Internal air mass ($kg.s^{-1}$)

h_{a}^{e}: Enthalpy of air entering the node

h_{fum}^{s}: Enthalpy of air outing the node

Q: Heat source at node i

According to heat transfer mode, the following equations are adopted:

- The conductive conductance:

$$k_{i,j} = \frac{\lambda S}{e} \quad (2)$$

Where:

λ: Thermal conductivity

S: Surface of node

e: Characteristic thickness of material

- The convective conductance

$$h_c = hS \quad (3)$$

h:is the convection heat transfer

- The radiative conductance

$$h_r = \varepsilon . F . \sigma \left(T_j + T_i\right)\left(T_j^2 + T_i^2\right) \quad (4)$$

ε: Emissivity of the wall,

F: Form factor,

σ: Stefan Boltzmann constant ($5.67.10^{-8} m^{-2}.K^{-4}$)

Inside the roasting oven, the convective heat transfer coefficient is calculated using the following relation:

$$Nu = a(Gr.\Pr)^n = \frac{hD}{\lambda} \quad (5)$$

$$Gr = \frac{g\beta L^3 \Delta T}{\nu^2} \quad (6)$$

$$\beta = \frac{1}{T} \quad (7)$$

$\Pr$ is the Prandtl number, $g = 9.81(N/kg)$ is gravity intensity. β is the Coefficient of thermal expansion of the fluid, L is the Characteristic length, ΔT is Temperature difference between the wall and the fluid (°C). For $10^4 < GrPr < 10^9$, the coefficients a=0.59 and n=0.25 and for $10^9 < GrPr < 10^{13}$, the coefficients a =0.21 and n=0.4 [17]. For temperature range of 300-1500 K at 1 atm, correlations used to determine the air thermo physical properties are [18]:

Specific heat:

$C_p = 936.2 + 0.2 * T$ (kJ/kg.K) (8)

Thermal conductivity:

$\lambda = 0.000318 * T^{0.7775}$ (W/m.K) (9)

Kinematic viscosity:

$\nu = (0.00006 * T + 0.063 * T - 9.54) * 10^{-6}$ (m^2/s) (10)

Dynamic viscosity:

$\mu = 0.044 * 10^{-5} * T^{0.7775}$ (Kg/m.s) (11)

Density:

$\rho = \frac{353}{T}$ (kg/m^3) (12)

$\Pr = 0.68$ (13)

Outside the oven, the Mc Adam relationship is used to calculate the heat transfer convection coefficient [19].

$h_c = 5.7 + 3.8V$

(14)
Where V is the air velocity (m/s).
Radiant heat transfer coefficients are calculated by these expressions:

$$h_{r,sky} = \frac{\sigma(T_i^2 + T_{sky}^2)(T_i + T_{sky})}{\frac{1}{\varepsilon} + \frac{1}{F_{sky}} - 1} \quad (15)$$

is the radiant heat transfer coefficient with the sky.

$$h_{r,ground} = \frac{\sigma(T_i^2 + T_{grand}^2)(T_i + T_{grand})}{\frac{1}{\varepsilon} + \frac{1}{F_{grand}} - 1} \quad (16)$$

is the radiant heat transfer coefficient with the ground.
Where F_{ground} and F_{sky} are radiative form factor. In the case of a vertical wall, the radiative form factor F_{sky} verifies the expression
determineted by Ivanova et al. [20] and J. Ramirez et al. [21].

$$F_{sky} = \frac{3\pi + 2b}{2\pi(3 + b)} \quad (17)$$

Where, b is a function of the anisotropy of the sky. For an isotropic sky (b = 0), the radiative form factor corresponds to 0.5. To determine the temperature of the sky, we use the correlations given by Swinbank [22] and the temperature of ground [23].

$$T_{sky} = 0.0552 * T_{ext}^{1.5} \quad (18)$$

$$T_{grand} = T_{ext} + 2 \quad (19)$$

Table1 summarizes the thermophysical properties of Roasting oven construction materials.

Table 1.Materials thermophysical properties

Material	Heat capacity ($J.kg^{-1}.K^{-1}$)	Density ($m^3.kg^{-1}$)	Thermal conductivity ($W.m^{-1}.K^{-1}$)
Iron sheet	478	4700	70

2.3. Numerical Method

2.3.1. Discretization of equations

All internal walls exchange heat by conduction, convection and radiation with the environment. We get the following relation:

$$\rho_i v_i c_i \frac{\partial T_i}{\partial t} = k_{i,j}(T_j - T_i) + k_{i,int}(T_j - T_i)$$

With,

$$k_{i,int} = h_{i,int}$$

The outer walls exchange heat by the convection and radiation with the external environment. We get the following relation:

$$\rho_i v_i c_i \frac{\partial T_i}{\partial t} = k_{i,j}(T_j - T_i) + k_{i,ext}(T_{ext} - T_i) + k_{i,sky}(T_{sky} - T_i) + k_{i,grand}(T_{grand} - T_i) + \phi_{sun}$$

$$k_{i,j} = \frac{\lambda_{iron} \cdot S_{iron}}{e_{iron}} \; ; \; k_{i,ext} = h_{ci,ext} + h_{r,ext} \; ; \; k_{i,sky} = h_{r,sky} S_{i,ext} \quad k_{i,ground} = h_{r,ground} S_{i,ext}$$

T_{sky} : Sky temperature (K)

T_{ground} : ground temperature (K)

T_{ext} : Ambient temperature (K)

The discretization of these equations gives for the external walls:

$$\rho_i V_i C_i \frac{T_i^{t+\Delta t} - T_i^t}{\Delta t} = k_{i,j}(T_j^{t+\Delta t} - T_i^{t+\Delta t}) + k_{i,ext}(T_{ext} - T_i^{t+\Delta t}) + k_{i,sky}(T_{sky} - T_i^{t+\Delta t}) + \phi_{sun}$$

Which gives:

$$(1+\beta_{i1,i2}+\beta_{i1,ext}+\beta_{i1,sky})T_{i1}^{t+\Delta t} - \beta_{i1,i2}T_{i2}^{t+\Delta t} = T_{i1}^t + \beta_{i1,ext}T_{ext} + \beta_{i1,sky}T_{sky} + \beta_{i1,sun}$$ We generally have:

$$\beta_{i,j} = \frac{\Delta t * k_{i,j}}{\rho_i V_i * C_i}, \quad \beta_{i,sky} = \frac{\Delta t * k_{i,sky}}{\rho_i V_i * C_i}, \quad \beta_{i,ext} = \frac{\Delta t * k_{i,ext}}{\rho_i V_i * C_i},$$

$$\beta_{i,int} = \frac{\Delta t * k_{i,int}}{\rho_i V_i * C_i}, \quad \beta_{i,ground} = \frac{\Delta t * k_{i,ground}}{\rho_i V_i * C_i} \quad \beta_{i,sun} = \frac{\Delta t * \phi_{sun}}{\rho_i V_i * C_i}$$, and

Likewise at the internal walls, we have:

$$(1+\beta_{i,j}+\beta_{i,int})T_i^{t+\Delta t} - \beta_{i,j}T_j^{t+\Delta t} - \beta_{i,int}T_j^{t+\Delta t} = T_i^t \quad (20)$$

2.3.2 Resolution method

At the instant t_0, the temperatures of the different parts of the oven are initialized at the ambient temperature, and then the various heat transfer coefficients by conduction, convection and radiation are calculated. Using Gauss's method, we solve the system of algebraic equations (16, 17) to determine the new value of the temperatures of the different parts of the oven at the instant $t_0 + \Delta t$. Then, the new values obtained are compared to the old values. The difference between the new and old values must be less than the precision otherwise the old values are replaced by the new values until convergence is obtained. The convergence criterion is:

$$\frac{T^{t+\Delta t} - T^t}{T^{t+\Delta t}} \leq 10^{-3} \quad (21)$$

.

3. RESULTS AND DISCUSSIONS

3.1. Model Validation

In order to validate our mathematical model, we compared our numerical and experimental results obtained under the same conditions. This comparison concerned the internal and external temperatures of the oven. To do this, the oven is switched on and then off after 45 minutes of no-load operation. It is then left to cool for 45 minutes. Temperatures are recorded using k type thermocouples (precision: 1.5°C) connected to a datalogger with a tolerance of: 0.05% (read value) ± 1 ° C. Four tests were carried out in order to obtain an average. The experimental setup is illustrated in Fig. 3.

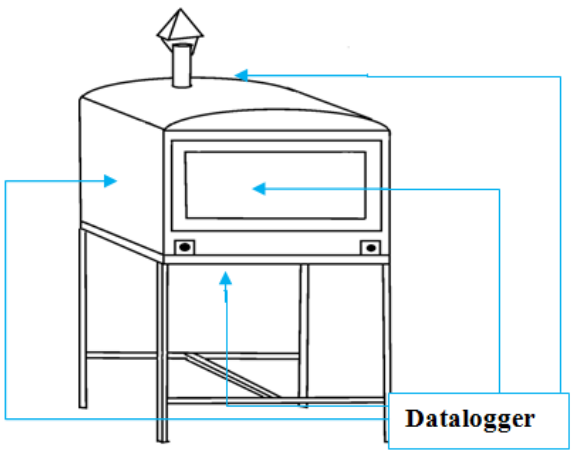

3Fig.3: Experimental setup

Meanwhile, based on the digital model, a computer program calculates the various desired temperatures. Figs. 4 and 5 show the internal and external comparison profiles respectively.

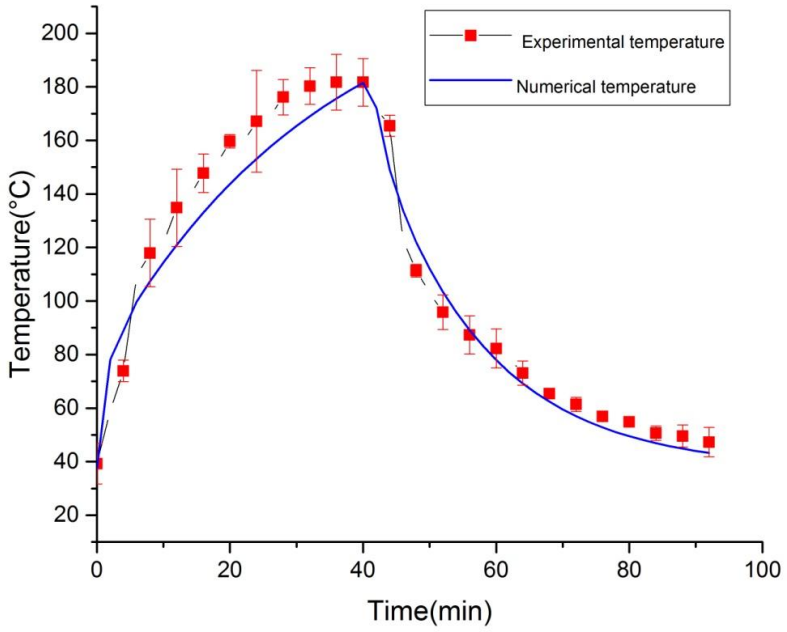

Fig.4. Comparison between numerical and experimental temperature oven cavity temperature profiles (wind speed: 3m/s, gas flow rate:9.10^{-3}kg/min, ambient temperature: 34.2°C.

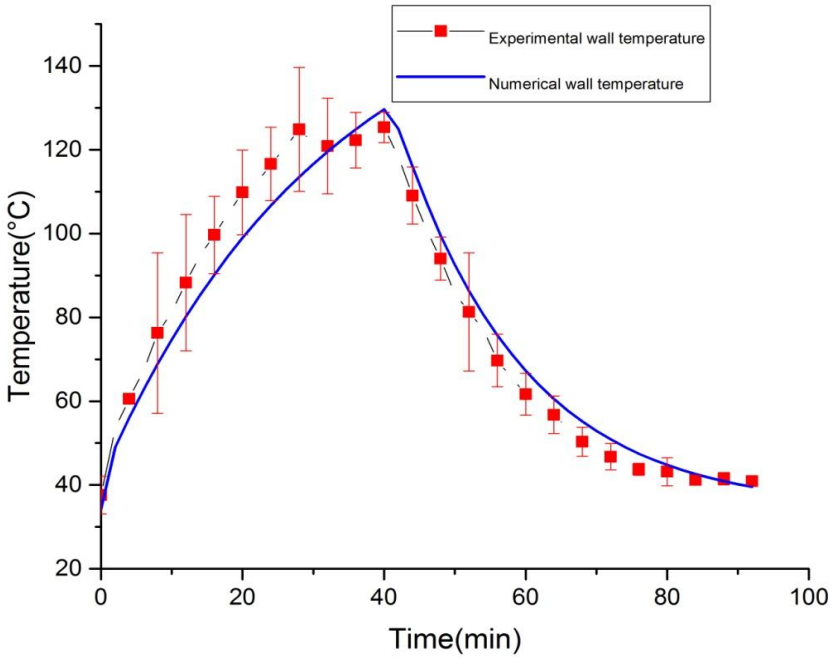

Fig.5. Comparison between numerical and experimental temperature profiles on lateral walls (wind speed: 3m/s, gas flow rate: 9.10^{-2}kg/min, ambient temperature: 34.2°C).

It is noted that on the whole of the two results, there is a good qualitative agreement between the numerical and experimental results. The relative maximum error $(\frac{|T_{num}-T_{exp}|}{T_{exp}}\times 100)$ between the numerical and experimental data is of the order of 9%. The deviations are mainly from the correlations used to approximate the heat transfer coefficients but also from the simplifying assumptions of the numerical model. On the other hand, we note that as soon as the burners are ignited, the internal temperature of the oven increases regularly until a peak (175°C) corresponding to the extinction of the flame (figure 3). The temperature then drops rapidly to ambient temperature. This rapid decrease is due to the absence of insulation in the oven causing a rapid transfer of heat to the external environment through the walls. It is also noted that the temperature profile of the external walls (figure 4) almost follows that of the internal air because of the thermal equilibrium.

3.2. Influence of extinction time on heat transfers

Fig.6 shows the evolution of the cavity temperature of the oven after three extinguishing of the flame, at t_1 = 30 minute, t_2 = 45 minute and t_3 = 60 minute.

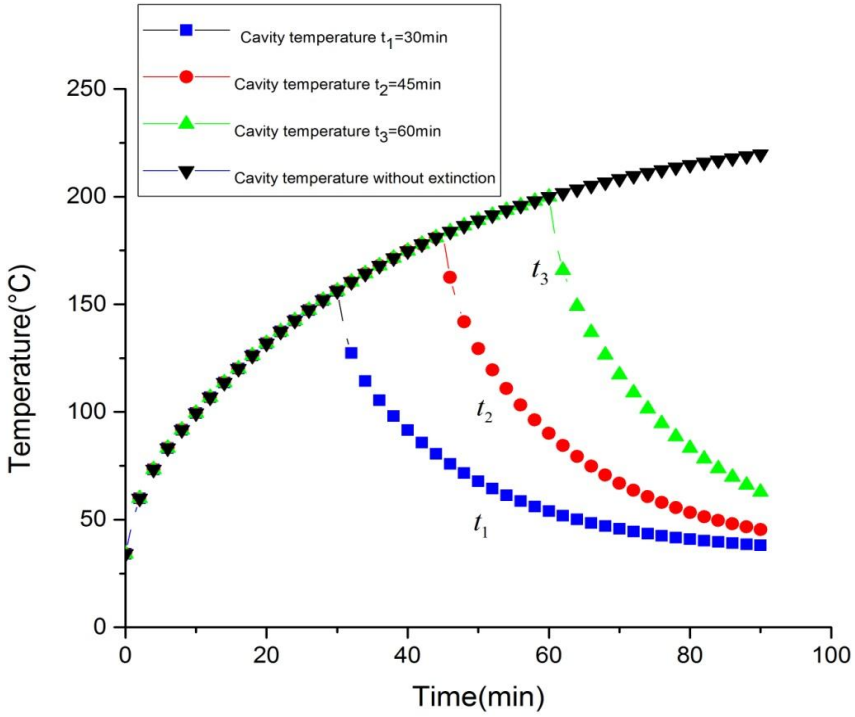

Fig.6. Evolution of the oven cavity temperature after 3 flame extinction (wind speed:3m/s; Ambient temperature:34.2°C; gas flow rate:9.10^{-3}kg/min).

As before, it is observed that the internal temperature of the oven increases regularly until the flame goes out, then drops rapidly to ambient temperature. This rapid drop in temperature is observed regardless of the extinction time. This result corroborates our previous observations and is due to the absence of insulation of the oven, resulting in the fact that the internal and external temperatures of the walls are confused as shown in fig.7.

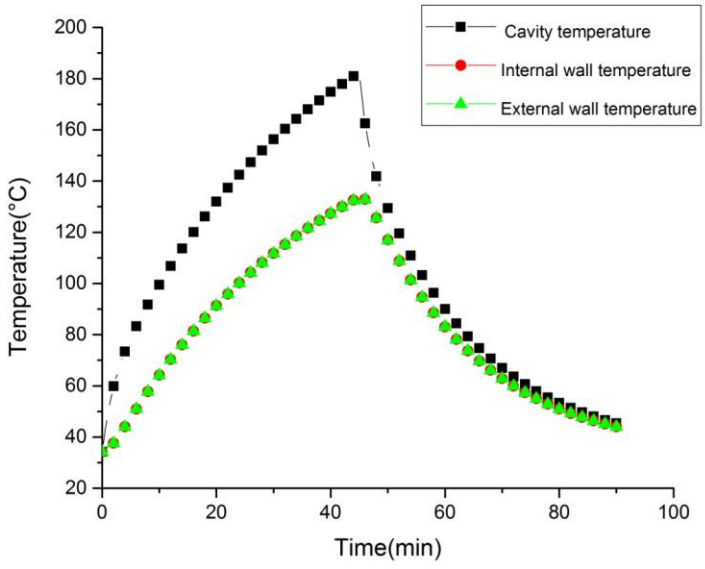

Fig.7. Evolution of the oven walls and cavity temperature (wind speed:3m/s; Ambient temperature:34.2°C; gas flow rate:9.10^{-3}kg/min).

3.3. Influence of gas flow rate on heat transfers

Fig. 8 shows the evolution of the oven cavity temperature as a function of the gas flow rate. In each case, the flame was

extinguished after 45 minutes of oven operation.

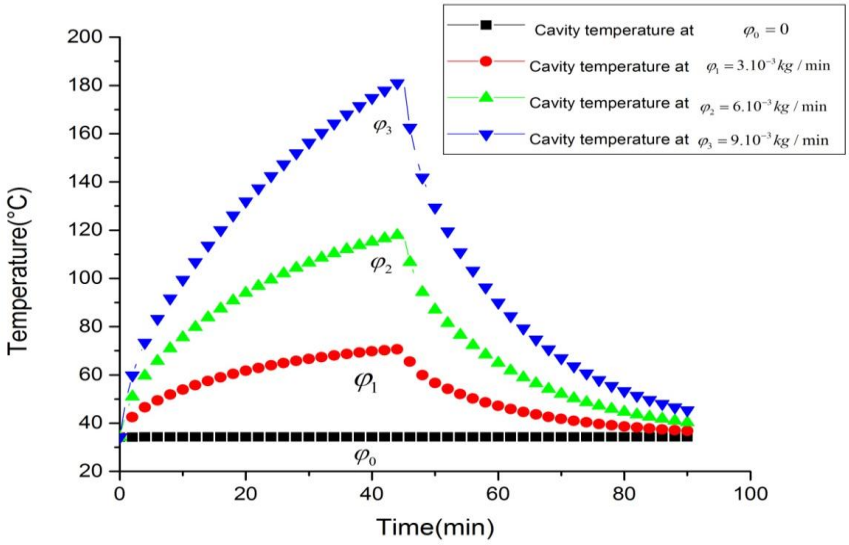

Fig.8.Oven cavity temperature versus gas flow rate (wind speed:3m/s; ambient temperature:34.2°C).

The results show that the more the gas flow increases, the more the temperature increases inside the oven. Indeed, the increase in gas flow rate increases the thermal power supplied by the burners, which leads to an increase in temperature. A zero gas flow rate consequently causes no increase in the temperature of the oven which remains at ambient temperature. We also observe that whatever the gas flow rate, the temperature drops rapidly after extinction of the flame to ambient temperature, which is in accordance with our previous observations.

3.4. Influence of wind speed on heat transfers

Fig. 9 shows the evolution of the oven cavity temperature as a function of wind speed. In each case, the flame was extinguished after 45 minutes of oven operation.

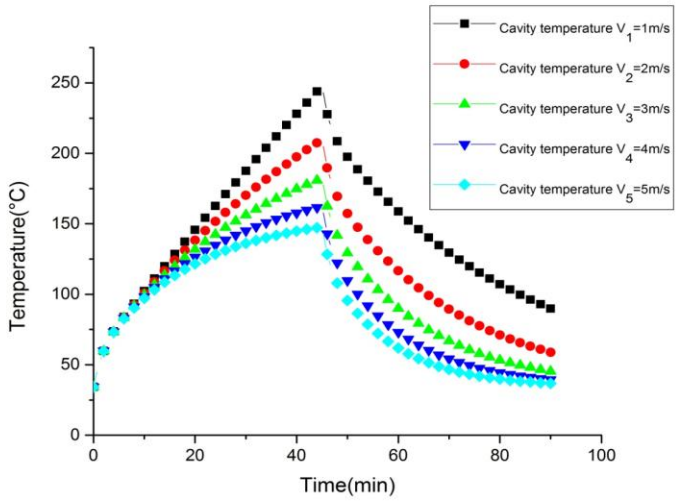

Fig. 9. Oven cavity temperature versus wind speed (ambient temperature: 34.2°C; gas flow

rate: 9.10^{-3}kg/min).

In general, it is observed that the effect of the wind greatly influences the transfers within the oven. We notice in fact that when the wind speed increases, the temperature drops inside the oven. This result is explained by the fact that the increase in the wind speed causes an increase in convective losses towards the external environment through the external wall of the oven, which lowers the internal temperature of the oven. This phenomenon is mainly observed after the first 15 minutes of operation of the oven when the temperature gradient between the oven cavity and the outside environment becomes significant. It is also noted that after 3 m/s, the losses are so great that the oven cavity temperature no longer varies and tend towards a limit value.

3.4. Influence of ambient temperature on heat transfers

Fig.10 shows the evolution of the oven cavity temperature as a function of ambient temperature. In each case, the flame was extinguished after 45 minutes of oven operation.

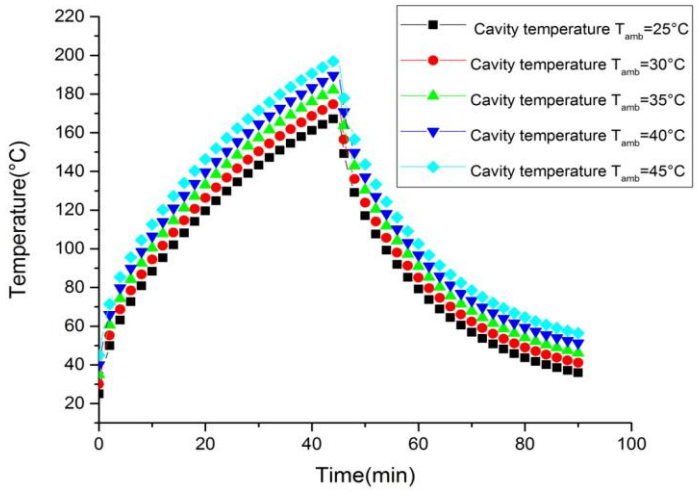

Fig.10. Oven cavity temperature versus ambient temperature (wind speed: 3m/s; gas flow rate: 9.10^{-3}kg).

It can be seen that increasing the ambient temperature improves transfers by increasing the oven cavity temperature. In fact, increasing the ambient temperature reduces the temperature gradient between the oven cavity and the outside environment, which reduces convective losses. It is this reduction in convective losses which causes this increase in temperature.

4. CONCLUSION

In this work, we carried out a numerical study of heat transfers in a typical Burkina Faso roasting oven. The numerical methodology is based on the nodal method and the equations obtained were discretized using an implicit finite difference scheme, then solved by the Gauss algorithm. The main results are summarized as follows:

- The increase in gas flow and the ambient temperature lead to an increase in the oven cavity temperature,
- The effect of wind is very important on transfers especially after the first 15 minutes of oven operation. Increasing the wind speed lowers the oven cavity temperature. After 3 m/s, the effect of the wind is no longer significant,
- After the flame has been extinguished, the oven cavity temperature drops rapidly to ambient temperature, which indicates poor thermal inertia of the oven. This rapid decrease is independent of the flame extinction time, gas flow rate, ambient temperature and wind speed.

These results make it possible to understand the thermal behavior of the oven and to identify its shortcomings, which will subsequently make it possible to carry out studies to improve the equipment.

REFERENCES

1. Gaël LS, Serge WI,Abdoulaye C, Drissa O, Xavier C, Belkacem Z. Experimental and numerical study of energy losses in a barbecue oven in Burkina Faso. Open journal of Energy Efficiency.2020; 9(1):31-52.
2. Serge WI, Kokou N, Abdoulaye C, Palm K, Gaël LS, David N. Experimental analysis of the thermal performance of a metal fired-wood oven. Iranian (iranica). journal of Energy and Environment.2020; 11(3):2025-2030.
3. Serge WI, David N, Abdoulaye C, Gaël LS, Drissa O, Joseph DB. Study and analysis of energy use efficiency of a local gas roasting oven. Journal of Energy Research and Review.2020; 6(4):30-37.
4. Gaël LS, Serge WI, Abdoulaye C, Drissa O, David N, Joseph DB. Modeling of Energy Savings Performed by a Barbecue Oven Isolated with Terracotta Bricks. Physical Science International Journal.2020; 24(5):8-21.
5. Serge WI, Gaël LS, Drissa O, Abdoulaye C, David N, Joseph DB. Numerical study of the performance of a double-insulated barbecue oven: implication for energy savings and thermal comfort. Physical Science Interntaional Journal.2020; 24(11):5-18.
6. Serge WI, Gaël LS, Drissa O, Abdoulaye C, David N, Joseph DB. Experimental study of charcoal savings achieved by an insulated oven with terracotta bricks: implications for the protection of forest resources. International. Journal of Environment and Climate Change.2021; 11(1):1-10.
7. Gaël, LS. Modélisation des phénomènes de transfert de chaleur dans un four isolé avec des matériaux locaux : application à l'optimisation énergétique des équipements de grillade de la viande. Thèse de Physique.Université Joseph Ki Zerbo.2020.
8. Rek Z, Rudolf M, Žun I, Strojniški V. Application of CFD simulation in the development of a new generation of heating oven. Journal of Mechanical Engineering (2012); 58,134-144. doi:10.5545/sv-jme.2011.163.
9. Pieter v, Ashim KD, Nguyen TA, Nico S, Bart MN. Computation of airflow effects on heat and mass transfer in a microwave oven. Journal of Food Engineering.2003; 2,3:181-190. doi:10.1016/S0260-8774(02)00456.
10. Davide P, Sauro P, Flavio M, Laura P. Heat and mass transfer in roast beef cooking. Temperature and weight loss prediction. Chemical Engineering Transactions.2015.
11. Melike SY, Kaymak EF, Ili C. Modeling of simultaneous heat and mass transfer during convective oven ring cake baking. Elsevier: Journal of Food Ingeneering. 2012; 111:289-298.
12. Uroš K, Leopold Š, Jure R. The validation of numerical methodology for oven design optimization using numerical simulations and baking experiments. Journal of Mechanical Engineering.2017;163(4):215-224.
13. Hachem ME. Stabilized Finite Element Method for Heat Transfer and Turbulent Flows Inside Industrial Furnaces.2009.
14. Hadi E, Akbar Z, Jafar SS,Mohamed Z,Ali A. Zonal modeling of radiative heat transfer in industrial furnaces using simplified model for exchange area calculation. Applied Modelling.2013;137:8004-8015.
15. Montrol T, Jacques J, Shihe X, Ronnie K, Marie LD, Aurélien M. Construction d'un modèle thermique nodal. *2eme* Congres De L'assocation Marocaine De Thermique Casablanca.2012.
16. Boyer H, Chabriat JP, Grondin-Perez B, Grondin-Perez C, Tourrand JB. Thermal building simulation and computer generation of nodal models. Building and Environment.1996; 31:207-214.
17. Sacadura JF. Initiation aux transfers thermiques. Edition Tech & doc, 6ème.2000.
18. Kshirsager MP,Vilas rk. A mathematical tool for predicting thermal performance of natural draft biomass cook stoves and identification of a new operational parameter. . Energy for Sustainable Development.2015; 93:188-201.
19. Adams M. Transmission de la chaleur. Dunod. Paris.1964.
20. Ivanova,S.M.Estimation of Background Diffuse Irradiance on Orthogonal surfaces under Partially Obstructed Anisotropic Sky Part I:Vertical Surfaces. Solar Energy.2013; 95:376-391.https://doi.org/10.1109/9.402235.
21. Ramirez-Faz J,Lopez-Luque R and Casares FJ. Development of Synthetic Hemispheric Projections Suitable for Assessing the Sky View Factor on Vertical Planes. Renewable Energy.2015;7:279-286. https://doi.org/10.1016/j.renene 2014.08.025.
22. Oudjedi S, Boubghal A, Braham CW, Chergui T and Belhamri A. Etude parametrique d'un capteur solaire plan à air destine au sechage. (Partie : 2). Revue des Energies Renouvelables.2008. SMSTS '08, Alger, 255.
23. Khaled, T., Mourad, H., Ali, M. Design and Modeling of a Photovoltaic thermal Collector for Domestic air Heating and electricity Production. ELSEVIER :Energy and Buildings.2013;59:21-28.

DEFINITIONS, ACRONYMS, ABBREVIATIONS

ρ_l : Density (kg.m^{-3})

V_i : Volume of node i

C_i : Material heat capacity (J/kg.K)

k_{ij} : Thermal conductance at nodes i and j ($W.K^{-1}$)

m_i : Mass of node i (kg)

h_{air}^{e} : Enthalpy of air entering the internal node ($J.kg^{-1}$)

h_{air}^{s} : Enthalpy of air outing the internal node ($J.kg^{-1}$)

Q_i : Heat source at node i (J)

m_{air}^{e} : Mass of air entering in the node i (kg)

m_{air}^{s} : Mass of air outing of the node i (kg)

λ_{air} : Thermal conductivity of air ($W.m^{-1}.K^{-1}$)

λ_{iron} : Thermal conductivity of iron sheet ($W.m^{-1}.K^{-1}$)

h_r : Radiative coefficient ($W.m^{-2}.K^{-1}$)

h_c : Convection heat transfer coefficient ($W.m^{-2}.K^{-1}$)

σ : Stefan Boltzmann constant ($5.67.10^{-8} m^{-2}.K^{-4}$)

F : Form factor

$T_{i,j}$: Temperature at nodes i and j (K)

T_{ext} : Ambient temperature (K)

T_{sky} : Sky temperature (K)

T_{ground} : Ground temperature(K)

S : Surface (m^2)

G_r : Grashof number

P_r : Prandtl number

N_u : Nusselt number

e_{iron} : Characteristic thickness (m)

ε : Wall Emissivity

V : Air velocity (m/s)

$\min$: Minutes